

Chapter 3

Evolution of the f Family Orbits in the Photo–Gravitational Sun–Saturn System with Oblateness

In chapter 2 we have analyzed PSS for values of C from $C = 1.0$ to admissible value of C . We have obtained different kinds of orbits: periodic, quasi–periodic and chaotic regions. Also, we have focused on two different family of orbits: Sun centered and Saturn centered orbits. We have analyzed the effect of C and q on both families of orbits. In this chapter we study Saturn centered simply symmetric retrograde periodic orbits known as f family periodic orbits. f family of periodic orbits play an important role in dynamics because it is used for patching of trajectory of satellite, that is, joining of two or more orbits to obtain a trajectory.

3.1 Introduction

[Dutt and Sharma(2012)] have analyzed the f family of orbits around smaller primary under RTBP for different systems. They have studied numerous systems in the ideal condition. [Winter (2000), Henon (1970), Douskos et. al. (2007), Dutt and Sharma (2011b)] have shown that the stability of periodic orbits of f family

is lost due to third–order resonances. The same phenomenon has been explicitly shown by [Perdiou et. al. (2012)]. [Pathak et. al. (2016a)] have analyzed Sun and Saturn centered periodic orbits with solar radiation pressure and Jacobi constant C as parameters and by considering actual oblateness of Saturn. They have found that there is a non–negligible effect of solar radiation pressure on the position and geometry of orbit of secondary body.

In this chapter \mathbf{f} family orbits and their stability for Sun–Saturn system is analyzed under the effect of solar radiation pressure. Here Sun is a source of radiation and Saturn is considered as oblate spheroid. So, actual coefficient of oblateness for Saturn is taken into account. For different values of mass reduction coefficient q , we have studied the \mathbf{f} family periodic orbits and the regions of quasi–periodic motion around Saturn in the photo–gravitational Sun–Saturn system in the framework of planar circular RTBP with oblateness. The location and nature of these orbits and size of the stability region of periodic orbits are studied using the numerical technique of Poincaré surfaces of section (PSS). It is observed that as Jacobi constant C increases, the number of islands in the PSS and consequently the number of periodic and quasi–periodic orbits increases. It is observed that as the perturbation due to solar radiation pressure decreases, the two separatrices come closer to each other and also come closer to Saturn. It is found that the eccentricity and semi–major axis of periodic orbits at both separatrices are increased by perturbation due to q .

3.2 Computational technique

Equations (1.4.12) through (1.4.16) are equations of motion of secondary body for the Sun–Saturn system, where mean motion n is given by equation (1.4.17) and mass reduction factor q is given by equation (1.4.18). Throughout this chapter the oblateness coefficient A_2 is taken as actual oblateness of Saturn whereas, q is taken as variable. The mass factor μ for the Sun–Saturn system is given by $\mu = \frac{m_2}{m_1 + m_2} = 0.0002857696$. Also according to equation (1.4.19), the oblateness coefficient is calculated as $A_2 = 6.59158 \times 10^{-11}$.

For constructing a PSS, the equations of motion (1.4.12) through (1.4.16) are integrated in (x, y) variables using a Runge–Kutta–Gill fourth order fixed step–size

integrator. By defining a plane, say $y = 0$, in the resulting three dimensional space, the values of x and \dot{x} can be plotted every time the particle has $y = 0$, whenever the trajectory intersects the plane in a particular direction, say $\dot{y} > 0$. It is noted that the resulting 3D space is reduced to a 2D subspace by considering a fixed value of the Jacobi constant. We have constructed PSS on the $x-\dot{x}$ plane. The initial values were selected along the Ox -axis. Time interval is taken as 0.001 which is the step size for Runge–Kutta–Gill fourth order integration method.

A PSS contains discrete points of trajectories. For a given q , selection of C is not arbitrary. By setting $y = 0$ and $\dot{y}^2 > 0$ in to equation (1.5.46), the resulting inequality defines the permissible regions on the PSSs. Thus, we eliminate the possibility of excluded region for secondary body between Sun and Saturn. This maximum value of C is considered as admissible value of C . We have analyzed the effect of solar radiation pressure on admissible value of C . For simplicity in writing the head rows of Table 3.1, solar radiation pressure, maximum value of C , value of C greater than admissible value of C , lower limit of excluded region, upper limit of excluded region and size of the excluded region are denoted by q , C_M , C , LER , UER and SER respectively. From Table 3.1 it is observed that as q decreases (i.e. perturbation due to solar radiation pressure increases), the maximum value of C decreases. Thus, due to solar radiation pressure range of Jacobi constant decreases. Any further increment in C gives excluded region for secondary body.

From Table 3.1 and Figure 3.1 it is clear that size of excluded region increases as C increases beyond admissible value of C . Figure 3.1 shows size of excluded region for different solar radiation pressure q . The maximum value of C corresponding to $q = 0.9$ is 2.807. Any further increase in the value of C , say 2.808 will give negative \dot{y}^2 for x in the range $[0.9290, 0.9510]$. This is the excluded region for the secondary body for $q = 0.9$. Figure 3.2 shows PSS corresponding to $C = 3.018$. Here we ignore solar radiation pressure (i.e. $q = 1$). Figure 3.3 shows one major island whose center gives Saturn centered simply symmetric retrograde periodic orbit at $x = 0.987101$ which is elliptic in shape. This orbit is categorized as **f** family orbit. **f** family periodic orbits being elliptic in shape, it is possible to obtain its semi-major axis and eccentricity.

Table 3.2 shows the analysis of **f** family periodic orbits. From each pair of q and C , we have calculated center of island x , semi-major axis a , eccentricity e , diameter D

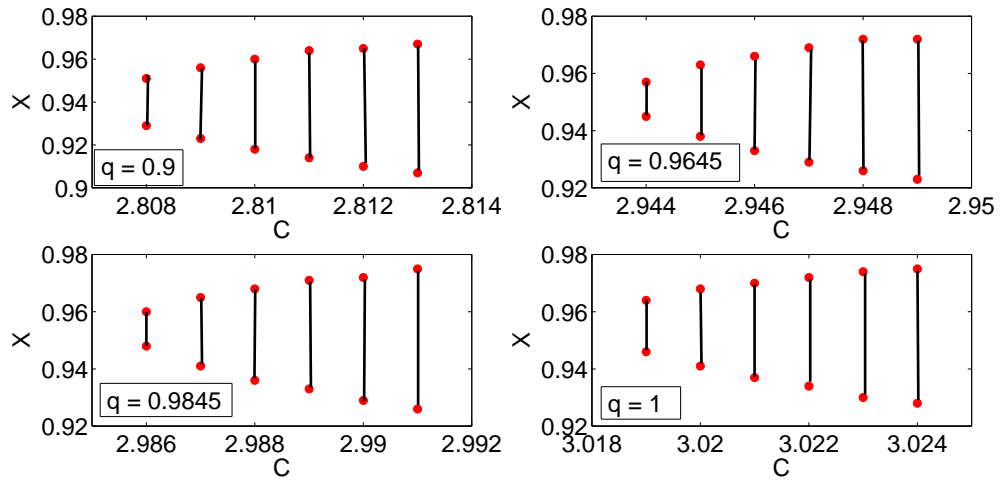


Figure 3.1: Excluded region for different solar radiation pressure q .

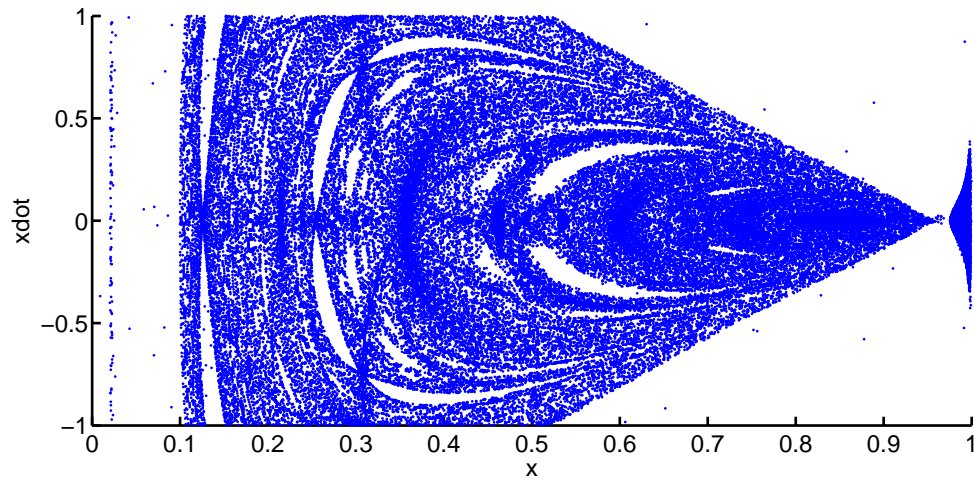


Figure 3.2: PSS for $C = 3.018$, $q = 1$.

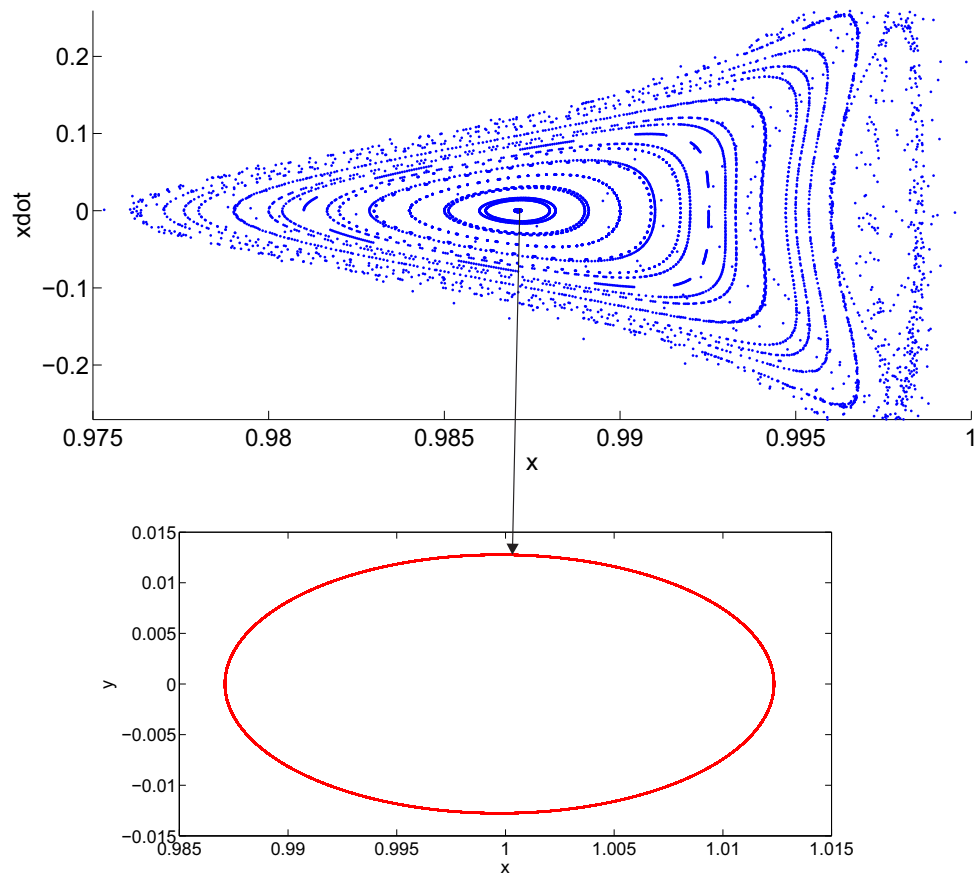


Figure 3.3: PSS for $C = 3.018$, $q = 1$, periodic orbit located at center of the island at $x = 0.987101$.

Table 3.1: Range of Jacobi constant for different solar radiation pressure q .

q	C_M	C	LER	UER	SER
1	3.018	3.019	0.946	0.964	0.018
		3.020	0.941	0.968	0.027
		3.021	0.937	0.970	0.033
		3.022	0.934	0.972	0.038
		3.023	0.930	0.974	0.044
		3.024	0.928	0.975	0.047
0.9845	2.985	2.986	0.948	0.960	0.012
		2.987	0.941	0.965	0.024
		2.988	0.936	0.968	0.032
		2.989	0.933	0.971	0.038
		2.990	0.929	0.972	0.043
		2.991	0.926	0.975	0.049
0.9645	2.943	2.944	0.945	0.957	0.012
		2.945	0.938	0.963	0.025
		2.946	0.933	0.966	0.033
		2.947	0.929	0.969	0.040
		2.948	0.926	0.972	0.046
		2.949	0.923	0.972	0.049
0.9	2.807	2.808	0.929	0.951	0.022
		2.809	0.923	0.956	0.033
		2.810	0.918	0.960	0.042
		2.811	0.914	0.964	0.050
		2.812	0.910	0.965	0.055
		2.813	0.907	0.967	0.06

(which is difference between two end points of \mathbf{f} family orbit on Sun–Saturn line) and the period of \mathbf{f} family orbit T . The upper case letters L , R and A represent, respectively, the left tip, the right tip and the amplitude ($R - L$) of the island whose center x gives \mathbf{f} family periodic orbit.

Table 3.2: Analysis of \mathbf{f} family periodic orbits for given pairs of (q, C) .

q	C	x	a	e	D	T	L	R	A
1	2.800	0.56455	1.0022	0.43694	0.8705	6.27	0.5438	0.5770	0.0332
	2.795	0.55940	1.0021	0.44204	0.8816	6.27	0.5396	0.5792	0.0396
	2.790	0.55435	1.0021	0.44706	0.8917	6.28	0.5470	0.5590	0.0120
	2.785	0.54935	1.0021	0.45202	0.9017	6.28	0.5487	0.5500	0.0013
	2.780	0.54440	1.0020	0.45690	0.9116	6.28	0.525	0.559	0.034
0.9645	2.800	0.63620	0.9220	0.31052	0.7038	6.26	0.6324	0.6390	0.0066
	2.795	0.62960	0.9209	0.31052	0.7038	6.28	0.6290	0.6302	0.0012
	2.790	0.62315	0.9198	0.32305	0.7299	6.28	0.6213	0.6253	0.0040
	2.785	0.61685	0.9188	0.32912	0.7422	6.28	0.6130	0.6236	0.0106
	2.780	0.61065	0.9177	0.33500	0.7554	6.28	0.6060	0.6140	0.008
0.9345	2.800	0.72165	0.8834	0.18435	0.5123	6.22	0.6972	0.7400	0.0428
	2.795	0.71240	0.8814	0.19280	0.5316	6.23	0.6853	0.7334	0.0481
	2.790	0.70345	0.8793	0.20111	0.5495	6.23	0.6752	0.7250	0.0498
	2.785	0.69480	0.8773	0.20909	0.5662	6.24	0.6679	0.7165	0.0486
	2.780	0.68645	0.8754	0.21680	0.5826	6.24	0.6658	0.7070	0.0412

From Table 3.2 it is observed that for a given C , as q decreases, the location of \mathbf{f} family periodic orbits move towards Saturn, which supports the fact that solar radiation pressure acts opposite to the gravitational force. It is also observed from Table 3.2 that for a given C , as q decreases, semi-major axis a , eccentricity e and diameter D of \mathbf{f} family periodic orbits decrease. Thus, it is concluded that due to perturbation of solar radiation pressure, size of \mathbf{f} family periodic orbits decrease. It is also observed from Table 3.2 that for a given C , as q decreases, semi-major axis a , eccentricity e and diameter D of \mathbf{f} periodic orbits decrease. This shows that due to perturbation of solar radiation pressure, size of \mathbf{f} family periodic orbits decrease.

Table 3.3: Analysis of \mathbf{f} family periodic orbits.

q	C	x	a	e	D	T	L	R	A
	2.600	0.40000	1.0011	0.60048	1.2000	6.281	0.3940	0.4000	0.0060
	2.700	0.47339	1.0015	0.52744	1.0536	6.278	0.4687	0.4758	0.0072

Continued on next page

Table 3.3 – continued from previous page

q	C	x	a	e	D	T	L	R	A
	2.800	0.56455	1.0022	0.43694	0.8705	6.272	0.5438	0.5770	0.0332
	2.900	0.68880	1.0041	0.31455	0.6222	6.249	0.6652	0.7111	0.0458
	2.910	0.70450	1.0044	0.29920	0.5915	6.239	0.6836	0.7254	0.0418
	2.930	0.73920	1.0056	0.26566	0.5218	6.220	0.7124	0.7580	0.0456
	2.950	0.77960	1.0075	0.22714	0.4414	6.175	0.7568	0.7980	0.0412
	2.970	0.83000	1.0120	0.18114	0.3410	6.050	0.8109	0.8501	0.0392
	2.975	0.84520	1.0142	0.16807	0.3108	5.973	0.8290	0.8622	0.0332
	2.980	0.86220	1.0177	0.15436	0.2768	5.860	0.8401	0.8770	0.0369
	2.985	0.88160	1.0234	0.14036	0.2374	5.638	0.8610	0.8940	0.0330
	2.990	0.90470	1.0349	0.12770	0.1914	5.200	0.8940	0.9107	0.0167
	2.995	0.93334	1.0648	0.12550	0.1337	4.100	0.9297	0.9400	0.0103
	3.006	0.97585	1.2361	0.21160	0.0482	1.200	0.9559	0.9860	0.0301
	3.010	0.98117	1.3009	0.24660	0.0368	0.900	0.9614	0.9934	0.0320
	3.014	0.98465	1.3649	0.27930	0.0303	0.700	0.9713	0.9948	0.0235
	3.018	0.98710	1.4302	0.31045	0.0249	0.492	0.9753	0.9960	0.0207
	2.570	0.39587	0.9374	0.57770	1.1981	6.280	0.3786	0.4120	0.0334
	2.670	0.46929	0.9486	0.50540	1.0507	6.277	0.4456	0.4906	0.0450
	2.770	0.56060	0.9590	0.41570	0.8684	6.267	0.5399	0.5811	0.0412
	2.870	0.68530	0.9701	0.29410	0.6197	6.245	0.6637	0.7073	0.0436
	2.890	0.71800	0.9729	0.26270	0.5540	6.300	0.6930	0.7386	0.0456
0.9845	2.910	0.75555	0.9764	0.22700	0.4795	6.200	0.7340	0.7757	0.0417
	2.930	0.80075	0.9812	0.18510	0.3892	6.200	0.7775	0.8221	0.0446
	2.950	0.86120	0.9924	0.13400	0.2688	5.900	0.8363	0.8771	0.0408
	2.970	0.96090	1.1171	0.14160	0.0721	1.990	0.9540	0.9646	0.0106
	2.975	0.97360	1.1905	0.18340	0.0474	1.174	0.9540	0.9838	0.0298
	2.980	0.98040	1.2595	0.22260	0.0346	0.780	0.9646	0.9911	0.0265
	2.985	0.98455	1.3269	0.25884	0.0275	0.555	0.9730	0.9940	0.0210
	2.443	0.33585	0.8428	0.60140	1.3042	6.280	0.3211	0.3470	0.0259
	2.543	0.39855	0.8672	0.54050	1.1785	6.276	0.3777	0.4155	0.0378

Continued on next page

Table 3.3 – continued from previous page

q	C	x	a	e	D	T	L	R	A
	2.643	0.47370	0.8893	0.46750	1.0283	6.273	0.4514	0.4900	0.0386
	2.743	0.56810	0.9101	0.37610	0.8399	6.268	0.5487	0.5903	0.0416
	2.843	0.69995	0.9319	0.24960	0.5761	6.235	0.6796	0.7200	0.0404
	2.860	0.72995	0.9363	0.22130	0.5170	6.215	0.7058	0.7483	0.0425
	2.880	0.77100	0.9427	0.18330	0.4350	6.200	0.7493	0.7890	0.0397
	2.900	0.82250	0.9519	0.13760	0.3325	6.100	0.8043	0.8409	0.0366
	2.920	0.90170	0.9819	0.08480	0.1763	4.940	0.8960	0.9048	0.0088
	2.943	0.98125	1.2328	0.20510	0.0297	0.618	0.9694	0.9900	0.0206
	2.180	0.22650	0.6523	0.65260	1.5027	6.284	0.2150	0.2390	0.0240
	2.280	0.27231	0.6965	0.60890	1.4108	6.283	0.2583	0.2877	0.0294
	2.380	0.32535	0.7367	0.55830	1.3048	6.282	0.3110	0.3390	0.0280
	2.480	0.38755	0.7737	0.49910	1.1805	6.282	0.3664	0.4062	0.0398
	2.580	0.46220	0.8080	0.42820	1.0308	6.279	0.4432	0.4821	0.0389
0.9345	2.680	0.55585	0.8409	0.33940	0.8442	6.278	0.5318	0.5773	0.0455
	2.780	0.68645	0.8754	0.21680	0.5826	6.276	0.6658	0.7070	0.0412
	2.800	0.72170	0.8835	0.18430	0.5123	6.300	0.6976	0.7423	0.0447
	2.820	0.76310	0.8927	0.14680	0.4299	6.200	0.7419	0.7803	0.0384
	2.840	0.81560	0.9054	0.10170	0.3264	6.100	0.7982	0.8333	0.0351
	2.860	0.89900	0.9417	0.05090	0.1649	4.800	0.8980	0.9000	0.0020
	2.880	0.97591	1.2109	0.19230	0.0331	0.720	0.9660	0.9895	0.0235

In Table 3.3, for each arbitrary selected values of q , we have displayed the numerical estimates of x , a , e , T , L , R and A for different permitted values of C . It is clear that for a given q , as C increases location of periodic orbit moves towards Saturn. Diameter D of \mathbf{f} family periodic orbits decrease as C increases. Figure 3.4 shows that the location x of \mathbf{f} family orbits move towards Saturn and diameter D decreases as C increases for a given q . From Table 3.3 and Figure 3.5 it can be noticed that a increases with C up to certain value of C and then shows a sudden increment in a . For instance, for $q = 1$ and $C = 2.995$, \mathbf{f} family periodic orbit is located at $x = 0.93334$. Semi-major axis of this orbit is 1.0648, whereas, \mathbf{f} family periodic orbit corresponding to $q = 1$ and $C = 3.006$ is located at $x = 0.97585$ has

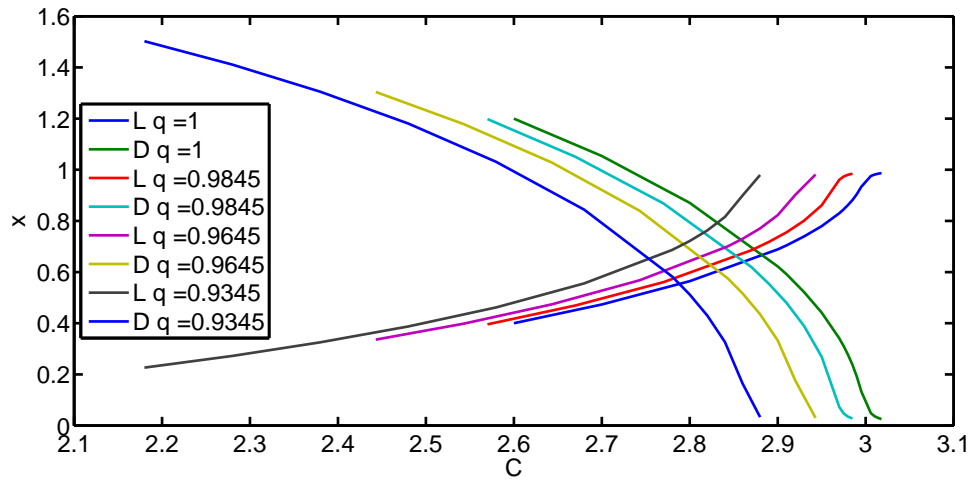


Figure 3.4: Location and diameter of f family periodic orbits.

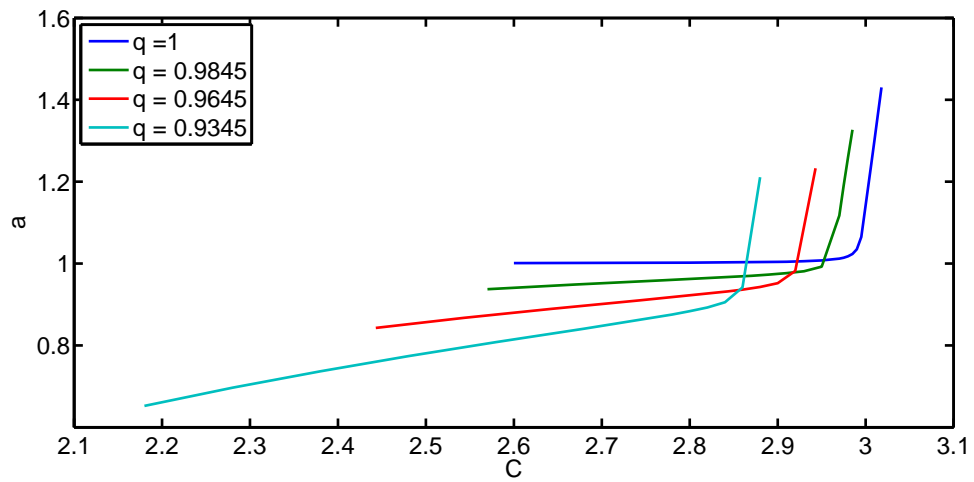


Figure 3.5: Semi-major axis of f family periodic orbits.

semi-major axis 1.2361 which is clearly a sudden increment in semi-major axis.

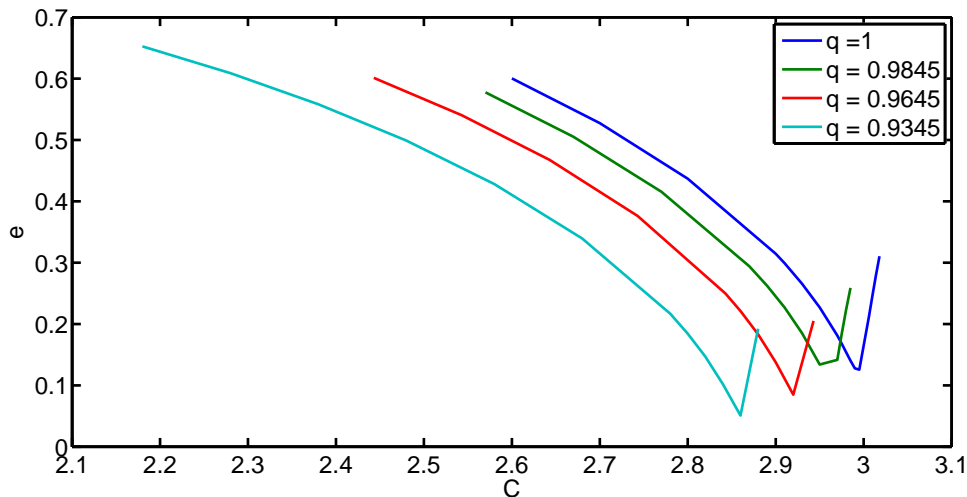


Figure 3.6: Eccentricity of \mathbf{f} family periodic orbits.

From Figure 3.6 it is observed that, for each q , eccentricity e decreases up to certain value of C and then increases suddenly as C increases. For instance, for $q = 1$, $C = 2.995$ \mathbf{f} family periodic orbit is at $x = 0.93334$. Eccentricity e of this orbit is 0.1255, whereas, \mathbf{f} family periodic orbit corresponding to $q = 1$, $C = 3.006$ is located at $x = 1.2361$. Eccentricity e of this orbit is 0.2116 which shows sudden increment in eccentricity.

Each point in the island around its center corresponds to a quasi-periodic orbit. The largest of these islands is the one with the maximum amplitude of oscillation that are still stable. The regular regions of PSS are defined by a periodic orbit surrounded by an area of quasi-periodic orbits. The regular regions can be interpreted as regions of stability in the sense that outside them the motion is certainly unstable (chaotic) and inside them the motion is in general stable.

Figures 3.7–3.10 give the size of the stability region for $q = 1, 0.9845, 0.9645$ and 0.9345 , respectively. The left and right tips of the island are plotted by red and green curves, respectively. It is seen that in each figure there are two separatrices where stability of the periodic orbit is zero as the size of the island is zero at separatrix.

For each PSS corresponding to a given point (q, C) , we get two separatrices. We have analyzed the stability curve for three stages, which are divided by two separatrices. In the first stage, the quasi-periodic orbit oscillates around the periodic orbits in

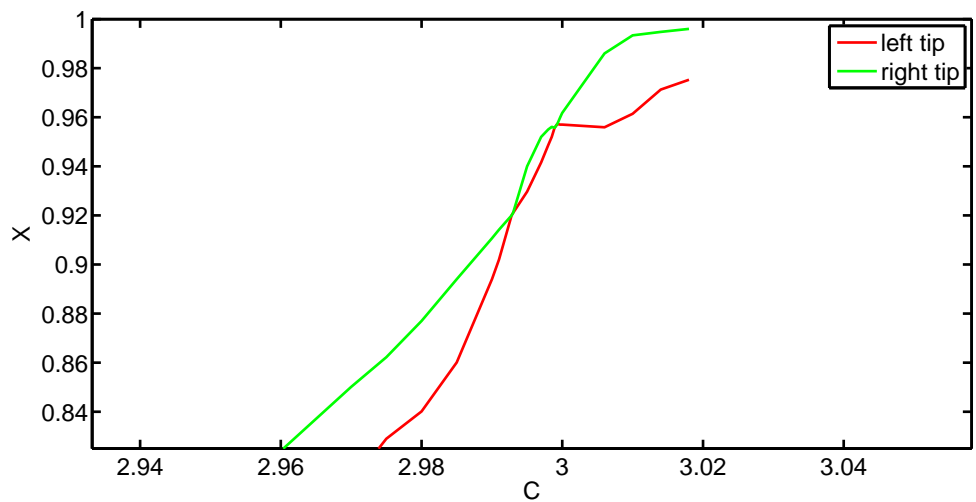


Figure 3.7: Stability of f family periodic orbits for $q = 1$.

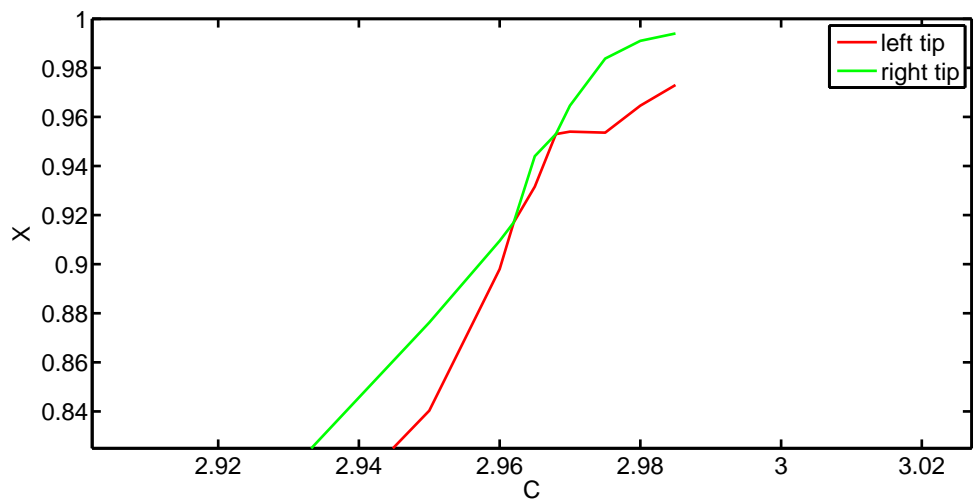


Figure 3.8: Stability of f family periodic orbits for $q = 0.9845$.

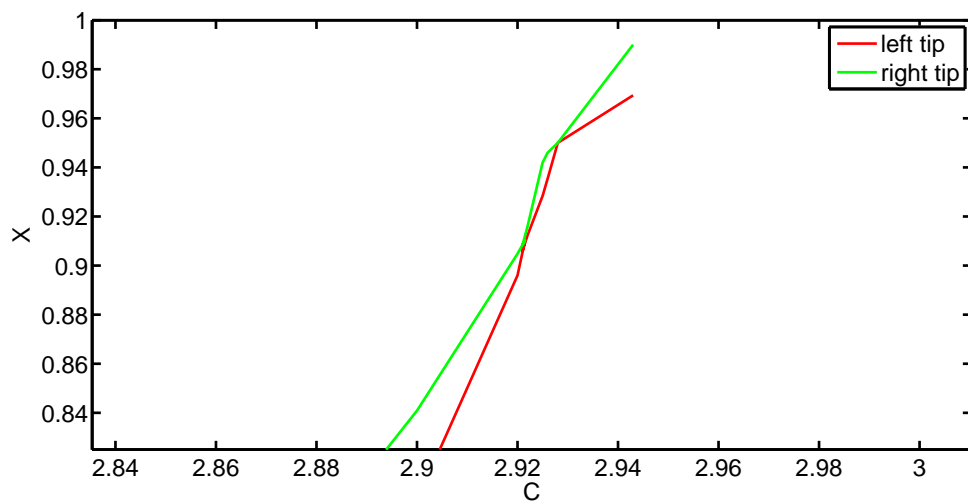


Figure 3.9: Stability of f family periodic orbits for $q = 0.9645$.

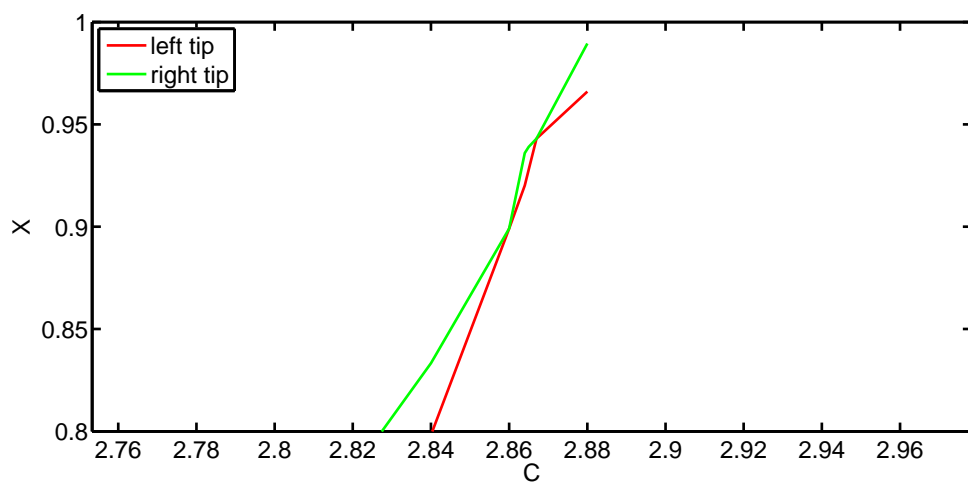


Figure 3.10: Stability of f family periodic orbits for $q = 0.9345$.

such a way that the farthest point from the Saturn in the line of conjunction is a pericenter. Stability of periodic orbit decreases up to first separatrix. At the first separatrix stability becomes zero as island disappears. In the second stage, island reappear and consequently the stability increases. Then size of the island starts decreasing up to second separatrix where again the island disappears. In the third stage, the quasi-periodic orbit oscillates around the periodic orbit in such a way that the closest point to the Saturn in the line of conjunction is pericenter. After second separatrix, island reappears and consequently the stability increases.

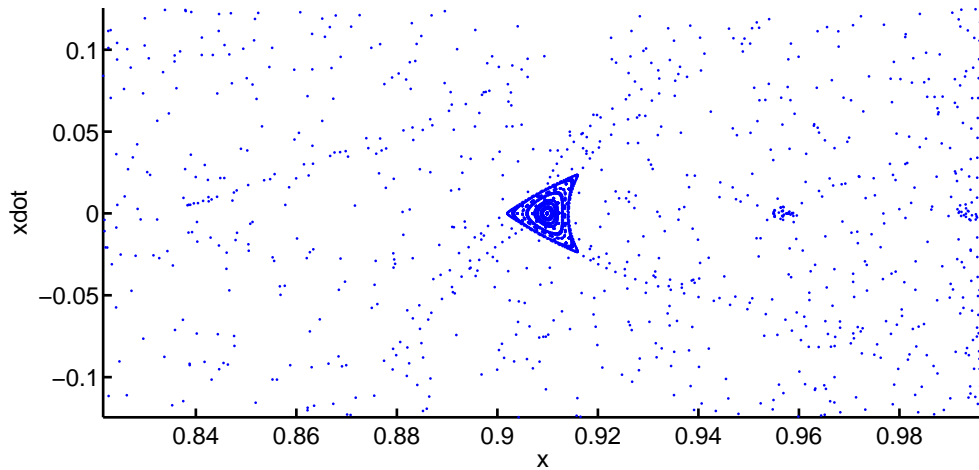


Figure 3.11: PSS of island for $C = 2.991$ and $q = 1$.

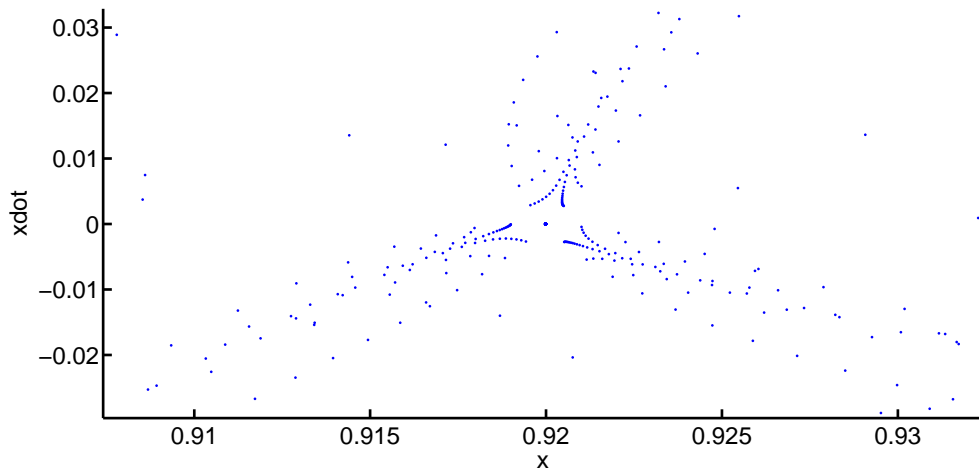


Figure 3.12: First separatrix for $C = 2.9928$ and $q = 1$.

From Figures 3.11–3.20, it can be noticed that there is a transition in the way the quasi-periodic orbit oscillates about the periodic orbit before and after the separatrix

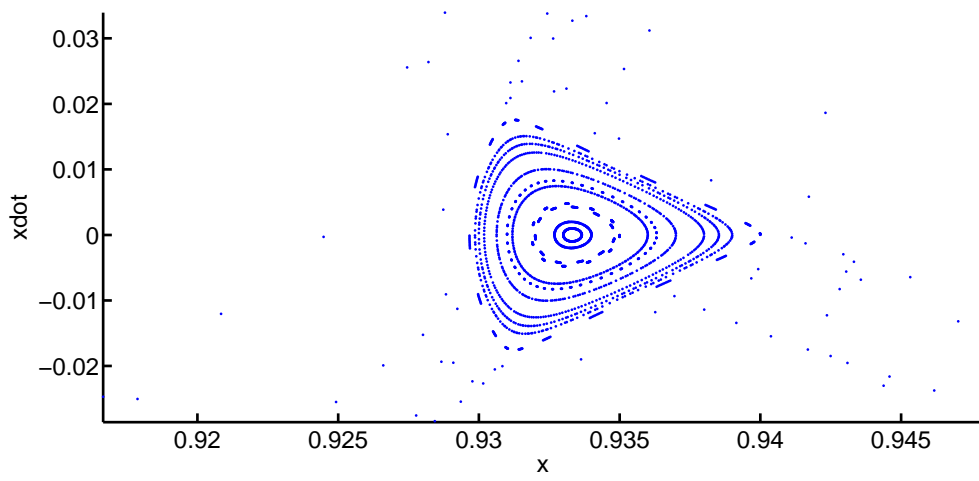


Figure 3.13: PSS of island for $C = 2.995$ and $q = 1$.

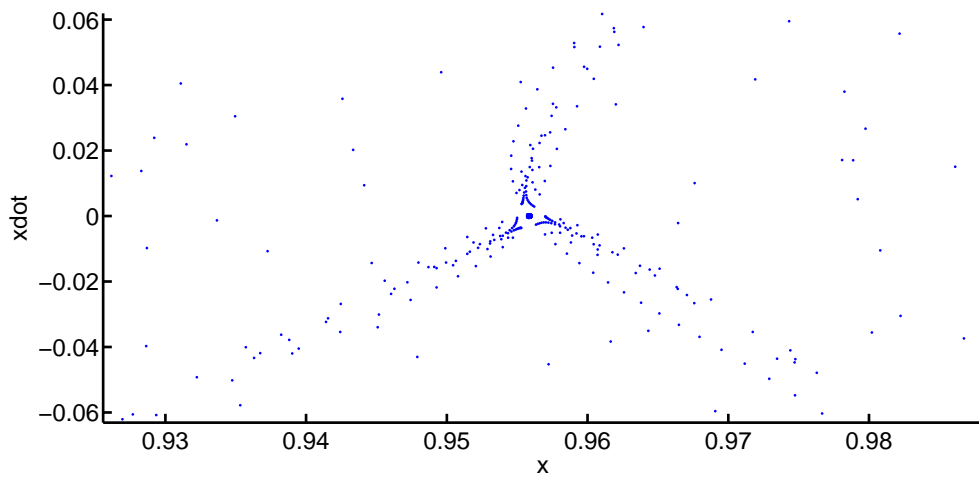


Figure 3.14: Second separatrix for $C = 2.999$ and $q = 1$.

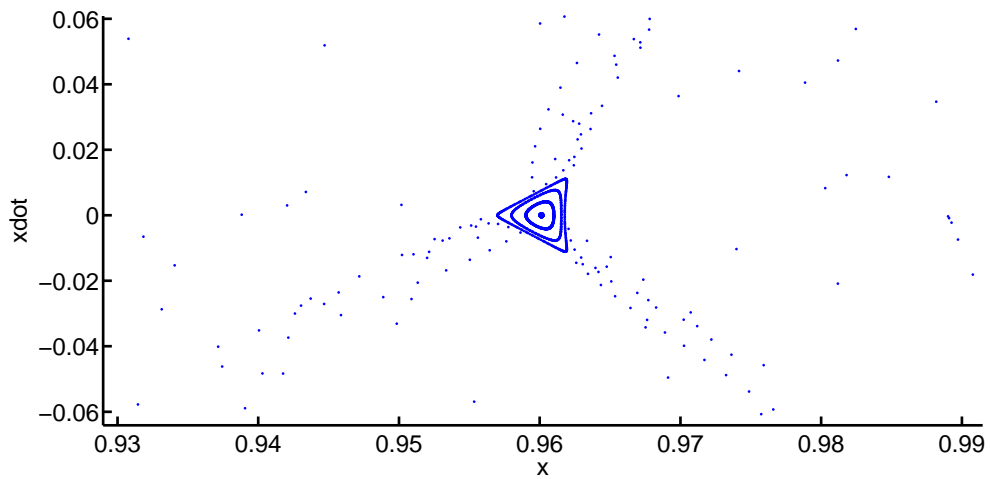


Figure 3.15: PSS of island for $C = 3.0$ and $q = 1$.

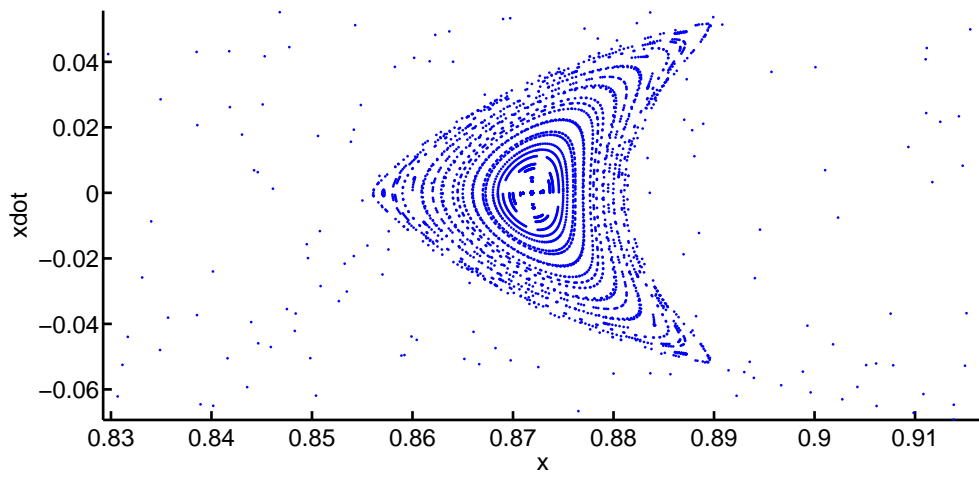


Figure 3.16: PSS of island for $C = 2.855$ and $q = 0.9345$.

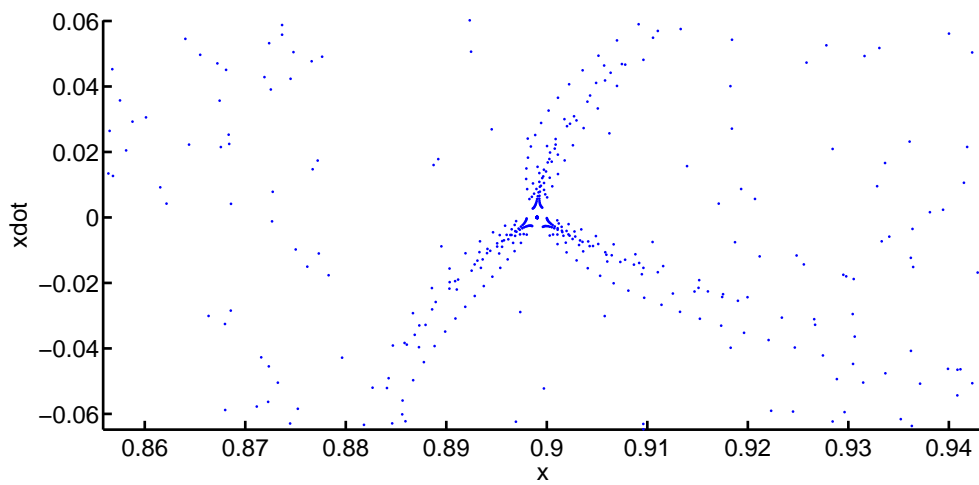


Figure 3.17: First separatrix for $C = 2.86$ and $q = 0.9345$.

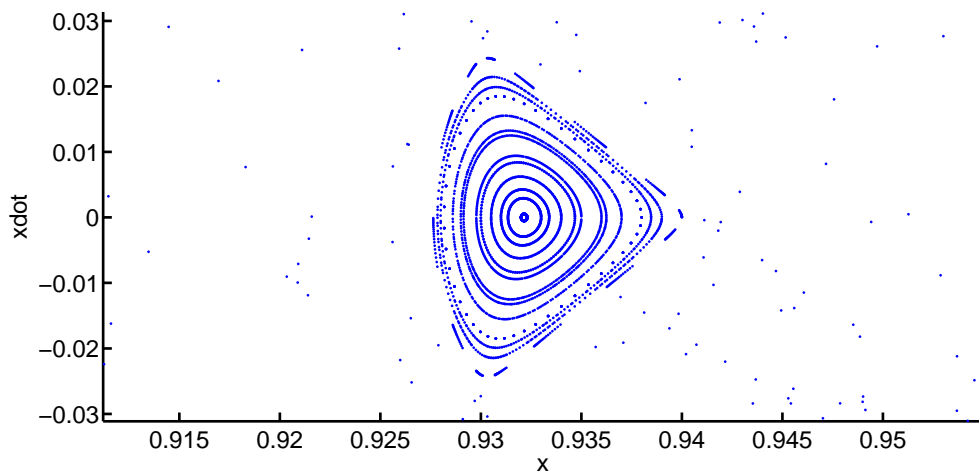


Figure 3.18: PSS of island for $C = 2.865$ and $q = 0.9345$.

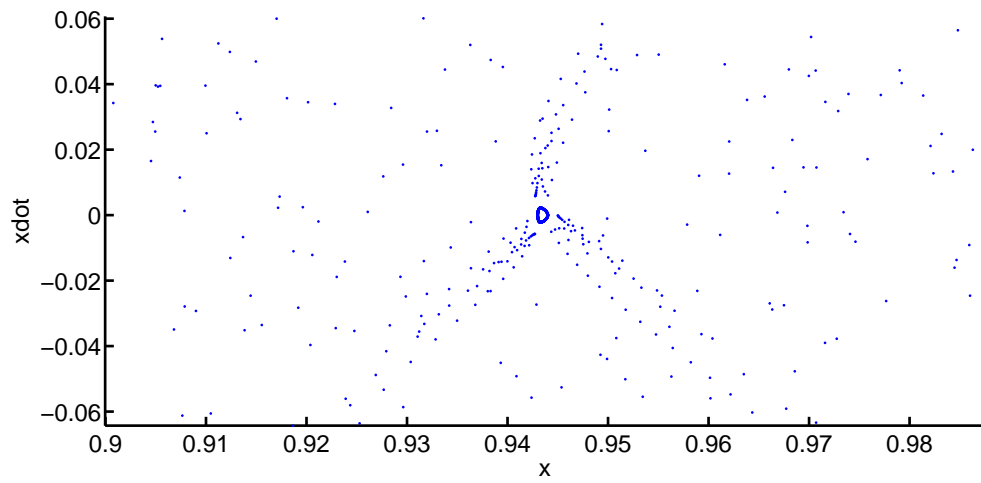


Figure 3.19: Second separatrix for $C = 2.867$ and $q = 0.9345$.

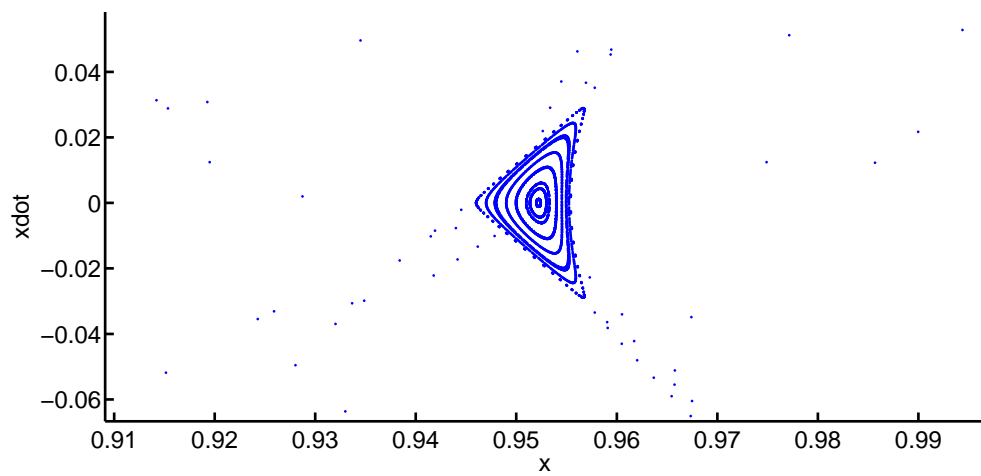


Figure 3.20: PSS of island for $C = 2.869$ and $q = 0.9345$.

due to third order resonance. The disappearance of the region of stability is caused by the intersection of the central periodic orbit and the unstable periodic orbit lying at the three corners of the triangular stability region [Dutt and Sharma (2011b)]. For $q = 1$, size of stability region increases as C increases in the range [2.6 2.9]. Stability is maximum at $C = 2.9$ and then decrease till first separatrix obtained at $C = 2.9928$. Again size of stability region increases and then decrease for very small interval of C and forms a loop as shown in figure 3.7. Second separatrix is obtained at $C = 2.999$ and again size of stability region increases.

Figures 3.11–3.15 show PSS of islands for $q = 1$ corresponding to $C = 2.991, 2.9928, 2.995, 2.999$ and 3.0 respectively. Figure 3.12 and Figure 3.14 are PSS of first and second separatrix for $q = 1$. Separatrices lie between two islands having opposite direction. Figures 3.11 and 3.13 are islands before and after first separatrix, respectively, having opposite direction. Similarly, Figures 3.13 and 3.15 are islands before and after second separatrix, respectively, having opposite direction.

For $q = 0.9345$ size of stability region increases for values of C in the range [2.18, 2.68]. For $q = 0.9345$ two separatrices are located at $C = 2.86$ and 2.867 . Figures 3.17 and 3.19 are PSS of separatrices for $q = 0.9345$. Figures 3.16 and 3.18 are islands before and after first separatrix. Thus, they have opposite directions. Similarly, figures 3.18 and 3.20 are island before and after second separatrix. So, they are in opposite directions.

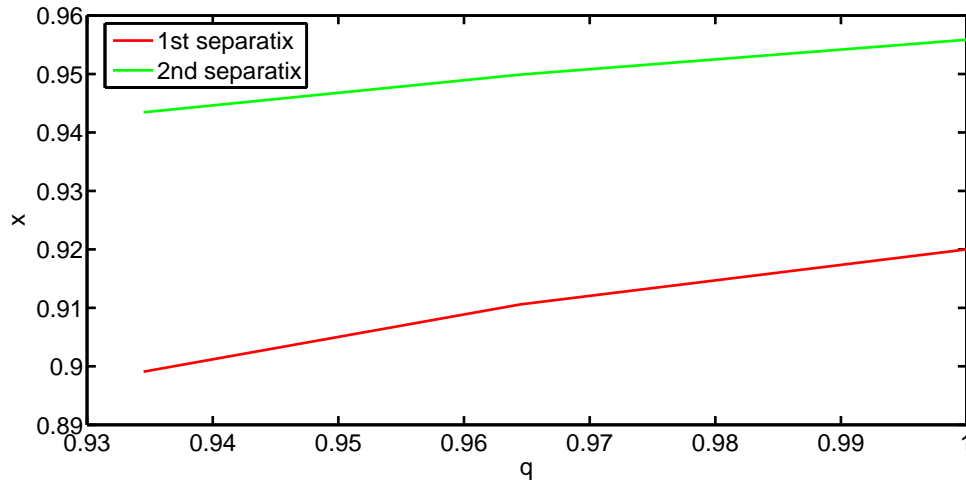


Figure 3.21: Location of separatrices for Sun–Saturn system as a function of q .

Reduction in q increases perturbation due to solar radiation pressure which affects

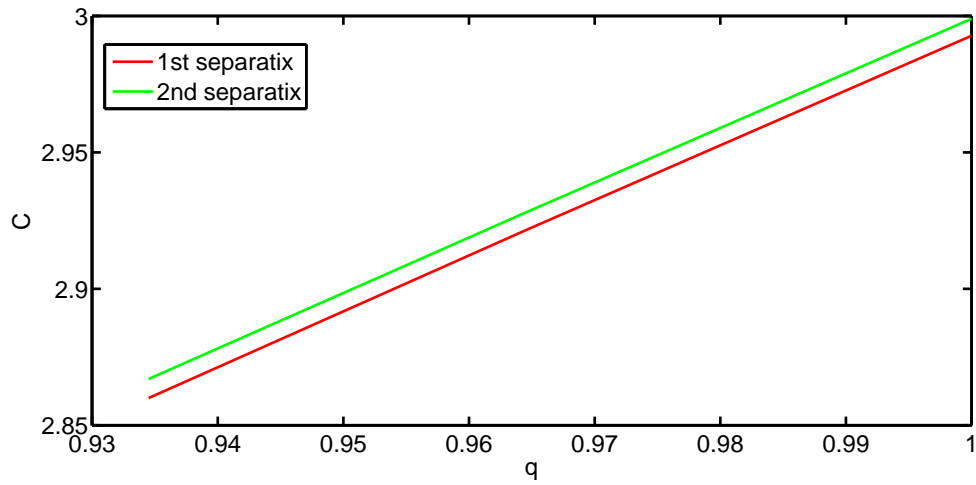


Figure 3.22: Value of C corresponding to the separatrices in Sun-Saturn system as a function of q .

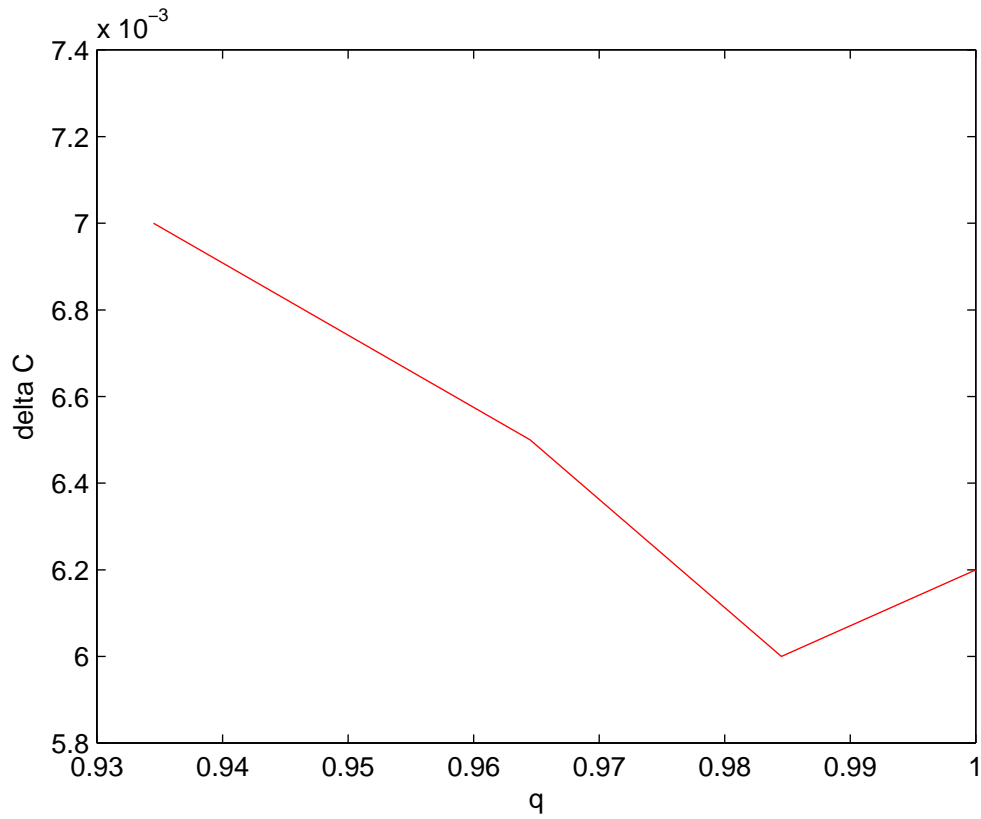


Figure 3.23: Difference between the values of C corresponding to the separatrices as a function of q .

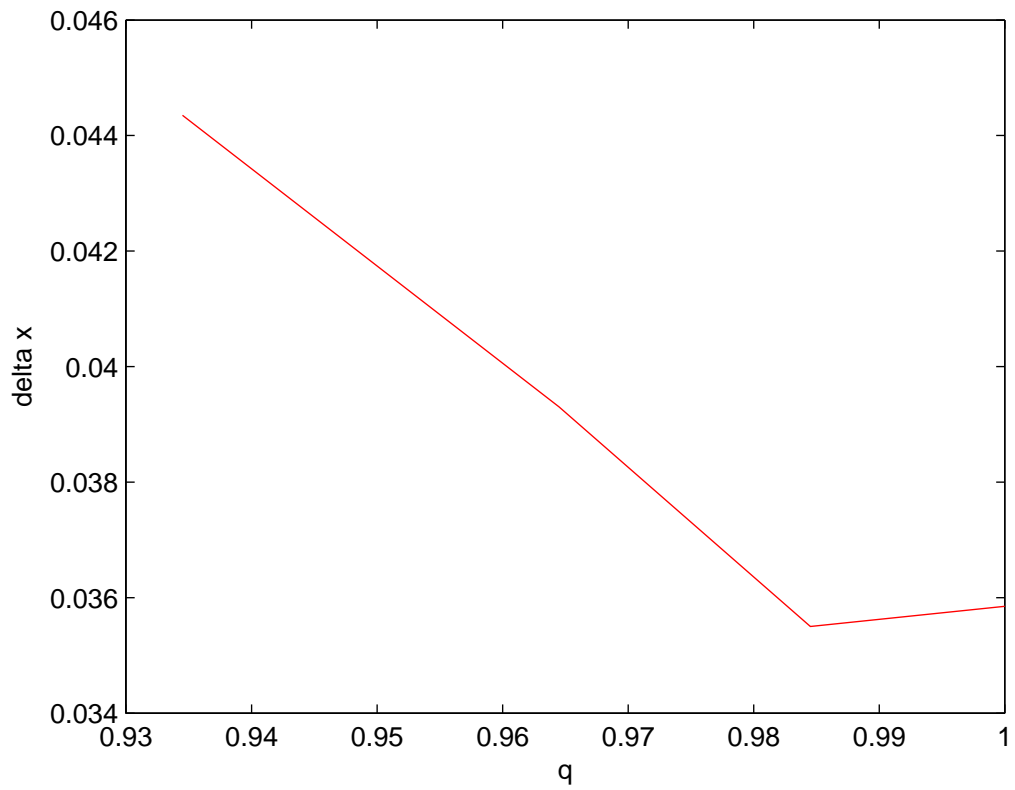


Figure 3.24: Distance between the location of two separatrices in Sun-Saturn system as a function of q .

Table 3.4: Analysis of periodic orbit at separatrices.

q	C	x	D	a	e
1.0000	2.9928	0.92000	0.1610	1.04760	0.1238
1.0000	2.9990	0.95585	0.0881	1.11897	0.1474
0.9845	2.9620	0.91725	0.1574	1.02272	0.1055
0.9845	2.9680	0.95275	0.0872	1.08780	0.1261
0.9645	2.9215	0.91060	0.1594	0.98936	0.0828
0.9645	2.9280	0.94990	0.0851	1.05420	0.1015
0.9345	2.8600	0.89910	0.1649	0.94180	0.0510
0.9345	2.8670	0.94345	0.0845	1.00360	0.0642

location, shape, size and stability of periodic orbits located at center of separatrix. Table 3.4 and Figure 3.21 show the variation in location of periodic orbits with respect to change in value of q at both separatrices. Red and green curves show variation in location of periodic orbit at first and second separatrix, respectively. It is observed that as q approaches 1, the location of periodic orbits at both separatrices moves towards Saturn. Figure 3.22 shows the variation in value of C corresponding to both separatrices as a function of q . Red and green curves correspond to first and second separatrices. It is clear that as q moves towards 1, value of C corresponding to both separatrices moves towards 3. Figure 3.23 shows difference between two Jacobi constants corresponding to first and second separatrices for given q . It is concluded that the difference between corresponding Jacobi constant decreases as q decreases up to 0.9845 and then increases slightly. Figure 3.24 shows distance between location of both separatrices for each q . It can be seen that the difference between location of two periodic orbits at both separatrices decreases as q drops to the value 0.9845 and then slightly increases. The effect of solar radiation pressure on the semi-major axis and eccentricity of the periodic orbits are shown in Figures 3.25 and 3.26. Red, green and magenta curves show behavior of location of periodic orbit at separatrices, its semi-major axis and eccentricity respectively. Figures 3.25 and 3.26 show the behavior of periodic orbits at first and second separatrices respectively. It is found that q is responsible for increment in e and a of periodic orbits at both separatrices.

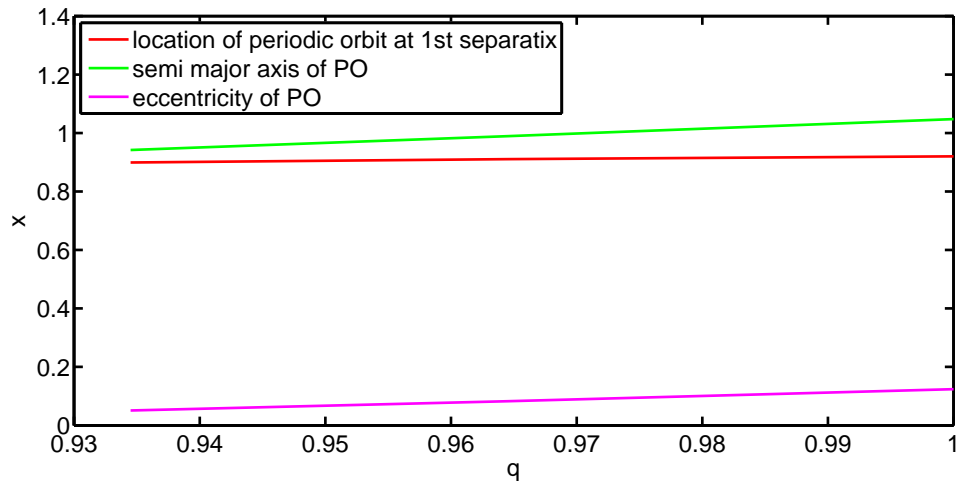


Figure 3.25: Location of periodic orbit at first separatrix, semi major axis and eccentricity of PO.

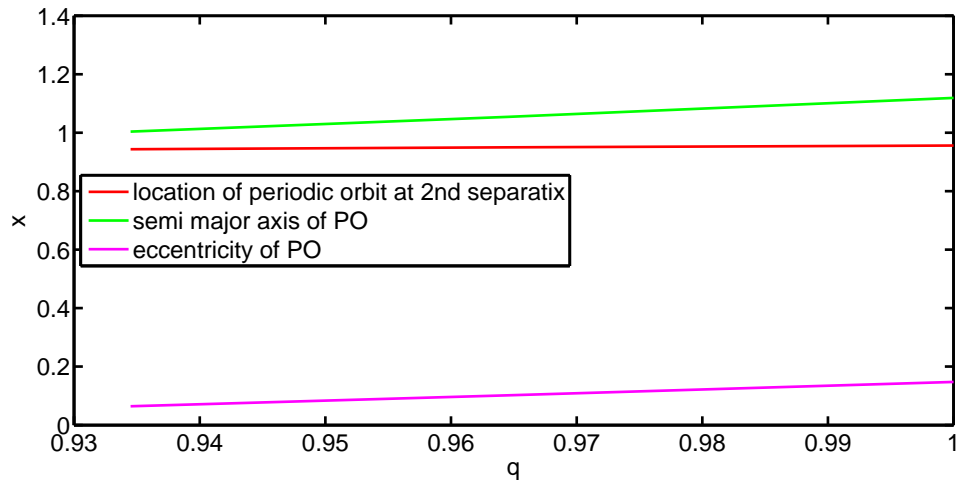


Figure 3.26: Location of periodic orbit at second separatrix, semi major axis and eccentricity of PO.

3.3 Conclusion

In the present chapter, we have analyzed the effect of radiation pressure and oblateness on \mathbf{f} family of periodic orbit (PO) in the Sun–Saturn system. It is observed that radiation pressure has significant influence on evolution of \mathbf{f} family of PO. As radiation pressure increases the admissible value of C decreases and PO shifts towards Saturn.

The geometric parameters of the orbits such as diameter, eccentricity and semi-major axis decrease. An increment in C increases the semi-major axis of \mathbf{f} family of periodic orbits, the eccentricity decreases up to certain value of C and then shows a sudden increase in its value. Diameters of these periodic orbits decrease slowly, but after certain value of C , there is a sudden decrement in value of diameter of periodic orbits. It is also observed that as solar radiation pressure decreases, the location of PO orbits at both separatrices moves towards Saturn.

As q moves towards 1, value of Jacobi constant corresponding to both separatrices moves towards 3. It is concluded that the difference between corresponding Jacobi constant decreases as q decreases up to 0.9845 and then increases slightly. It can be seen that the difference between location of two periodic orbits at both separatrices decreases as q drops to the value 0.9845 and then slightly increases. In other words, as the perturbation due to solar radiation pressure decreases, the two separatrices come closer to each other and also come closer to Saturn. It is found that the eccentricity and semi-major axis of periodic orbits at both separatrices are increased by perturbation due to solar radiation pressure. The evolution of the family of periodic orbits can be divided into three stages separated by two separatrices. There is a change in the direction of the islands around the periodic orbits before and after these separatrices. In other words, there is a change in the way the quasi-periodic orbits oscillate around the periodic orbits before and after these separatrices.